Programmable fabrication of monodisperse graphene nanoribbons via deterministic iterative synthesis

Jiangliang Yin[1†], Peter H. Jacobse[2,3†], Daniel Pyle[1], Ziyi Wang[2,3], Michael F. Crommie[2,3,4*] and Guangbin Dong[1*]

[1]Department of Chemistry, University of Chicago, Chicago, IL 60637, USA.

[2]Department of Physics, University of California at Berkeley, Berkeley, CA 94720, USA.

[3]Materials Sciences Division, Lawrence Berkeley National Laboratory, Berkeley, CA 94720, USA.

[4]Kavli Energy NanoSciences Institute at the University of California, Berkeley and the Lawrence Berkeley National Laboratory, Berkeley, CA 94720, USA.

KEYWORDS. graphene nanoribbons, iterative synthesis, surface-assisted cyclodehydrogenation, bond-resolved scanning tunneling microscopy, mono dispersity

ABSTRACT: While enormous progress has been achieved in synthesizing atomically precise graphene nanoribbons (GNRs), the preparation of GNRs with fully predetermined length and monomer sequence remains an unmet challenge. Here we report a fabrication method that provides access to structurally diverse and monodisperse "designer" GNRs through utilization of an iterative synthesis strategy, in which a single monomer is incorporated into an oligomer chain during each chemical cycle. Surface-assisted cyclodehydrogenation is subsequently employed to generate the final nanoribbons, and bond-resolved scanning tunneling microscopy is utilized to characterize them.

INTRODUCTION

Graphene nanoribbons (GNRs), defined as nanometer-wide strips of graphene, have recently attracted much attention because of their versatile electronic,[1-4] optical,[5] and magnetic[6,7] properties. This gives them potential for impactful future nanoelectronic, spintronic, photonic, sensing, quantum information processing, and energy conversion applications. The physical behavior of GNRs is dictated by their precise structure and can thus be tuned by altering parameters such as length, width, heteroatom doping, edge structure, defect incorporation, etc.[8-13] These parameters cannot be effectively controlled using top-down methods (such as e-beam lithography), but the development of chemistry-based bottom-up synthesis techniques has enabled fabrication of numerous atomically-precise GNR structures with engineered properties.[14-21] For example, the electronic bandgap and work function of GNRs have been shown to be readily tunable through chemical modification of molecular precursors.[22-24] GNR heterostructures have also been produced by covalently bonding GNR segments with different electronic characters, showing promise for use in electronic components such as field-effect transistors (FETs).[25-31] Topological engineering,[24,32-35] metallicity,[36] and magnetism[37,38] have all been successfully implemented in GNRs, further consolidating them as attractive nanomaterials for use in spintronic, qubit or memory devices.[39-46]

Despite this progress, however, it is still not possible to synthesize monodisperse GNRs having well-defined length or well-defined heterogeneous monomer sequence, important milestones that would enable new GNR functionality through flexible electronic interface engineering.[27,29,32,33] The problem is that bottom-up synthesis of GNRs currently relies mainly on conventional polymerization strategies (Figure 1a) and the resulting GNRs are invariably polydisperse and do not exhibit controlled monomer sequences beyond the simplest repeating subunits.[14-17] As such, bottom-up synthesized GNRs, while highly controlled in many aspects, thus still feature a range of different characteristics even for a single targeted structure. Elegant strategies, including hierarchical[29,47] and chain-growth polymerization[48] have been explored to partially alleviate this problem, but the selective, monodisperse preparation of GNRs having well-defined monomer sequence remains an unmet challenge.[21] In addition, GNRs from controlled assembly of more than two different types of building blocks are

elusive since current bottom-up strategies typically can only handle one or two different types of monomers during the polymerization process. Hence, while GNRs exhibiting irregular, non-periodic structural motifs have been predicted to have highly desirable properties in proposed nanoelectronic architectures,[31,49] there has so far been a lack of selective methods for their preparation. Herein, we describe our initial efforts of developing a general fabrication method for preparing diverse GNR structures assembled from multiple types of monomers and for yielding precisely controlled GNR sequence, length, and shape, which is enabled by a protecting-group-aided iterative synthesis (PAIS) strategy (Figure 1b).

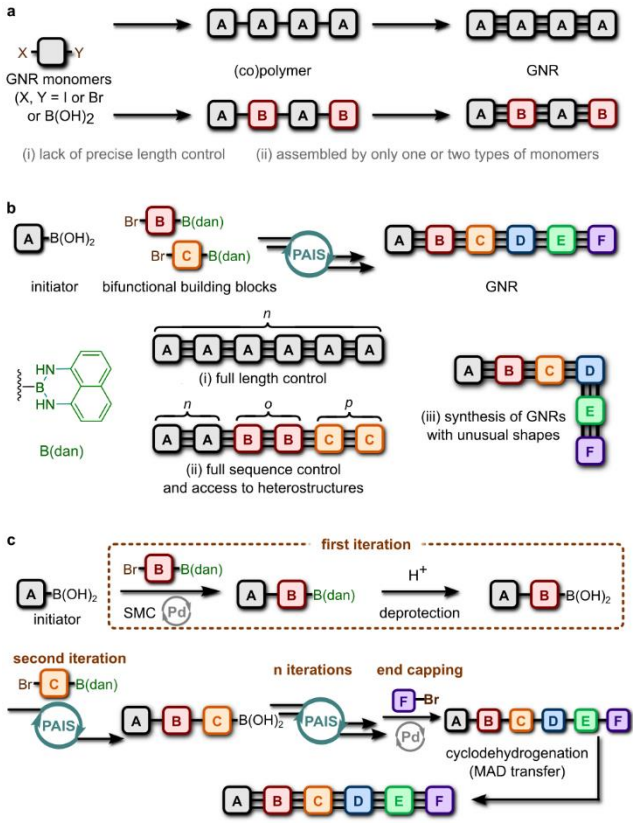

Figure 1. Bottom-up GNR synthesis strategies. (a) Conventional GNR synthesis via polymerization or co-polymerization of monomers. (b) This work: a new programmable fabrication strategy for obtaining structurally diverse and monodisperse "designer" GNRs, which is enabled by protecting-group-aided iterative synthesis (PAIS). dan: 1,8-diaminonaphthalene. (c) In this PAIS process the Suzuki–Miyaura coupling (SMC) and B(dan) deprotection constitute one operative iteration, and only one GNR monomer is introduced to the chain per iteration.

Inspired by state-of-the-art preparation strategies for oligonucleotides in which protecting groups play a key role in providing programmability and length control,[50,51] an intriguing question is that whether a similar approach can be adopted for the synthesis of GNR polymer or oligomer precursors. Considering the effectiveness of Suzuki–Miyaura coupling (SMC) in solution-phase GNR synthesis,[9,10,15,16,20,23] our PAIS strategy capitalizes on the use of bifunctional building blocks (BBBs) containing a halide and a masked boronic acid to achieve controlled iterative couplings (Figure 1c). Specifically, 1,8-diaminonaphthalene (dan) is used to protect the boronic acid group of our BBBs since [B(dan)] is stable and unreactive under SMC conditions and can be easily deprotected to reveal the reactive boronic acid moiety upon treatment with an acid, based on Suginome's seminal work.[52] We were motivated by the idea that a BBB containing both a bromo and B(dan) substituent could first couple with an initiating monomer (i.e., the "initiator") that only contains a boronic acid via SMC. Next, acid hydrolysis of the B(dan) moiety could be performed to deprotect the boronic acid, activating it for the next cross-coupling step. The resulting boronic acid intermediate could then be cross-coupled with the second (either the same or different) BBB for chain propagation. In this PAIS process the SMC and acid hydrolysis constitute one operative iteration, and *only one GNR monomer is introduced to the chain* per iteration. This is the key to realizing programmability and length/sequence control. The GNR polymer or oligomer chain can be terminated at any stage by SMC with an end-capping

monomer that only contains a bromo group. The final GNR product is then obtained through cyclodehydrogenation (CDH), either in solution or on-surface.

RESULTS AND DISCUSSION

Length control. To test this hypothesis, we first set out to prepare chevron-type GNRs[8] with exactly six repeating units (Figure 2a). To achieve this goal, we began with phenylboronic acid and performed six iterations of solution-based cross-coupling and hydrolysis with a chevron-type bifunctional building block (**BBB**$_{ch}$) prepared via borylation of the corresponding dibromo monomers and protection of the resulting boronic acid moiety with dan (for details, see Figure S1). SMC was realized in high yield with 1 mol% $Pd(dppf)Cl_2$ as catalyst, K_3PO_4 as base, H_2O as additive, and THF as solvent. In each SMC step, one chevron-type BBB was added to the oligomer; because the BBB contains an unreactive B(dan) group, no further coupling occurred afterwards. Hydrolysis was realized with HCl under N_2 atmosphere at 60 °C, which turned the unreactive B(dan) terminus into reactive $B(OH)_2$, effectively activating it for the next coupling rection with another BBB. The two-step SMC-deprotection process was iterated a total of six times to introduce six chevron repeating units, and the synthesis of the oligomer (GNR) precursor **pre-chGNR(6)** was completed by terminating coupling with PhBr.

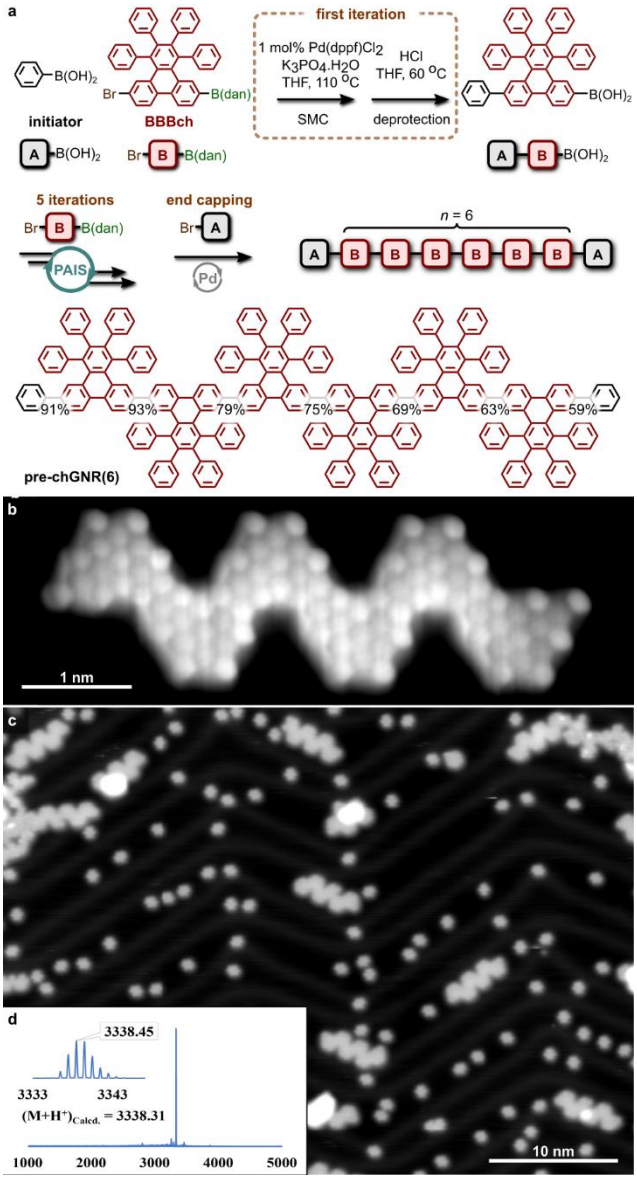

Figure 2. Length control: synthesis of **chGNR(6)**. (a) Synthesis of the oligomer (GNR) precursor **pre-chGNR(6)** demonstrating GNR length control. Yields for each iteration in the oligomer synthesis are provided at the corresponding connecting positions. (b) BRSTM image (constant height dI/dV at V = 0V) of **chGNR(6)**. (c) Large-scale STM topograph (V = –1.8V, I = 50pA) shows monodisperse **chGNR6** on Au(111) after CHD step. (d) MALDI-TOF-MS spectra of **pre-chGNR(6)**.

The resulting monodisperse **pre-chGNR(6)** sample was then transferred to a pre-cleaned Au(111) surface via the recently established matrix-assisted direct (MAD) transfer technique using pyrene as the matrix[53] (for details, see Supporting Information). The Au(111) sample was then heated to T_1 = 80 ºC for t = 10 h to sublime the pyrene matrix and induce diffusion of the polymers over the surface, followed by heating to T_2 = 360 ºC for t = 20 min to induce CDH of the oligomers into fully planar **ch-GNR(6)**. The resulting GNRs were characterized via bond-resolved scan tunneling microscopy (BRSTM) imaging, revealing the precise expected structure as shown in Figure 2b. Larger-scale STM scans (Figure 2c) show a highly monodisperse sample of chevron-type GNRs. The supermajority (> 80%) of GNRs observed on the surface have the expected chevron structure[8] with exactly six repeating units. Some defects were seen, such as an occasional incomplete CDH, as well as an occasional phenyl ring ejection, which are known to occur in on-surface CDH of chevron-type GNRs.[54,55] The overall GNR structure, however, is consistent with the desired **ch-GNR(6)**. The high monodispersity observed in our STM measurements was corroborated by MALDI-TOF mass spectra. As shown in Figure 2d, mass spectra reveal peaks corresponding precisely to the desired molecular weights of the GNR oligomer precursor. This suggests that the phenyl ejection defects observed in the surface-cyclized GNRs were introduced during the CDH step and are not likely to be present in the GNR precursor.

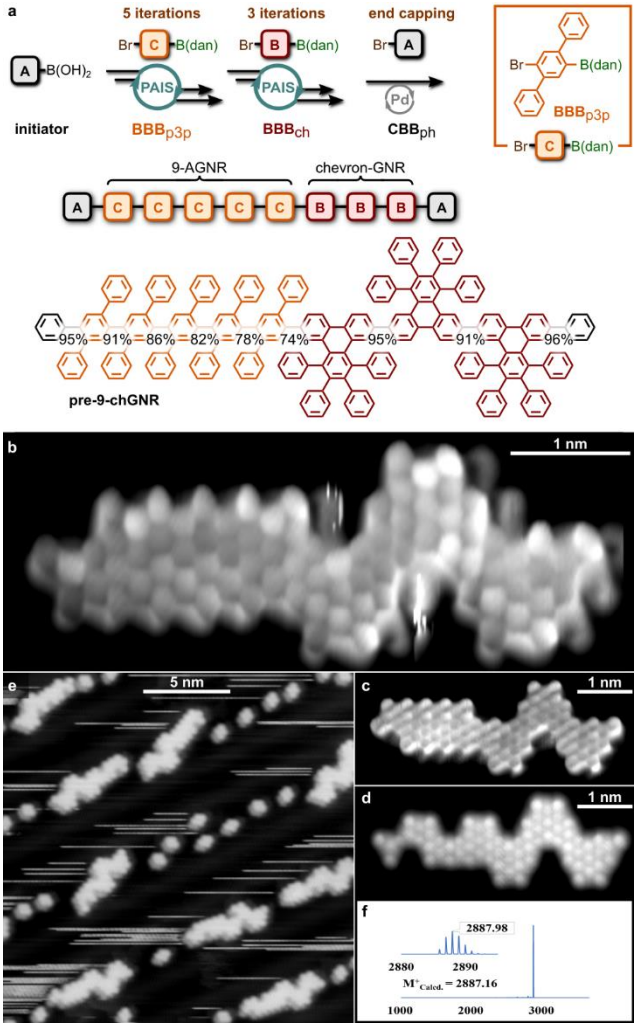

Figure 3. Heterostructure control: synthesis of **9-chGNRs**. (a) Synthesis of the oligomer (GNR) precursor **pre-9-chGNR** demonstrating a precise two-component GNR heterostructure. Yields for each iteration in the oligomer synthesis are provided at the corresponding connecting positions. (b) BRSTM image (constant height dI/dV at V = 0V) of **9-chGNR** after CHD. (c), (d) BRSTM images (constant height dI/dV at V = 0V) of **9-chGNRs** showing phenyl ejection defects. (e) Large-scale STM topograph (V = –0.8V, I = 50pA) shows monodisperse **9-chGNRs** on Au(111). **f** MALDI-TOF-MS spectra of **pre-9-chGNR** oligomer.

Heterostructure control. The PAIS method can also generate heterostructures with predefined monomer sequences of different building blocks in addition to precise length. To illustrate this point we have synthesized precise, monodisperse N=9 armchair/chevron GNR heterostructures (Figure 3a). The synthesis was started with the same phenylboronic acid initiator as before, after which five repeating units of para-terphenylene were added through five successive SMC/deprotection cycles utilizing the para-terphenylene building block (**BBB**$_{p3p}$). Three chevron monomers (**BBB**$_{ch}$) were then added to the chain afterwards, at which point the synthesis was completed by end-capping the oligomer with PhBr (Figure 3a). The resulting oligomer (GNR) precursor (**pre-9-chGNR**) was then transferred to the gold surface via the MAD-transfer protocol, after which CDH was performed to yield the final, fully planar **9-chGNR** heterostructure.

Figure 3b shows a BRSTM image of the final **9-chGNR** with the exact, intended GNR structure. We observe that this GNR heterostructure is prone to defect formation, such as phenyl ejection, upon on-surface CDH (Figures 3c, d). This is likely caused by the relatively free rotation of para-terphenyl groups around the GNR axis, leading to undesired stacking between neighboring phenyl rings and subsequent cleavage under CDH conditions. Regardless of these defects, the backbone of each GNR on the surface clearly shows the intended structure, as seen in larger-scale STM scans (Figure 3e). The MALDI-TOF mass spectra also reveals a set of sharp peaks at the intended molecular weights (Figure 3f), indicating that the observed defect formation is likely a consequence of the on-surface CDH process.

In order to explore the effectiveness of the PAIS strategy to create precise nonperiodic GNR structures with multiple interfaces, we fabricated a double heterojunction composed of two N=6 segments surrounding a single N=9 segment (Figure 4a shows a sketch of the intended structure). While polymers with ortho-terphenyl units are known to yield 9-AGNRs,[56,57] it was expected that an alternating sequence of the phenyl- and terphenyl units could cyclize into a 6-AGNR, analogous to previous work performed in solution.[23] To accomplish this the ortho-terphenyl bifunctional building block (**BBB**$_{o3p}$) and para-phenylene building block (**BBB**$_{p}$) were first coupled in an alternating manner for two cycles, and subsequently, five **BBB**$_{o3p}$ were incorporated into the chain, followed by adding another **BBB**$_{p}$ and **BBB**$_{o3p}$ units. After end capping, the **6/9/6-AGNR** heterojunction oligomer precursor (**pre-6/9/6-AGNR**), with 13 phenylene units in its backbone, was completed.

Figure 4b shows an STM image of the **pre-6/9/6-AGNR** oligomer precursors after MAD transfer to the surface (and before CHD). All GNR oligomers on the surface have the same structure, and in close-up images (Figure 4b, inset) a one-to-one correspondence between the observed pattern of lobes and the expected pattern of phenyl groups can be seen. CDH of this sample was performed on-surface to create the intended **6/9/6-AGNR** heterostructures. As illustrated by the BRSTM images in Figure 4c, the 9-AGNR segment cyclized well but isomerization via "flip" in the 6-AGNR regions occurred during CDH on surface. In these isomeric structures, successive terphenyl units have cyclized on opposite sides of the GNR axis after C–C σ bond rotation into conformationally isomeric forms of the oligomer. This was likely due to a slight steric repulsion between neighboring terphenyl units, which lowers the activation barrier for cyclization into the non-linear products. This is in contrast to the stereoregular cyclization observed in solution synthesis.[23] Nevertheless, the STM images of both cyclized and non-cyclized phases, as well as the MALDI-TOF mass spectra (Figure 4a inset), show that precise sequence and length control was achieved by the PAIS strategy.

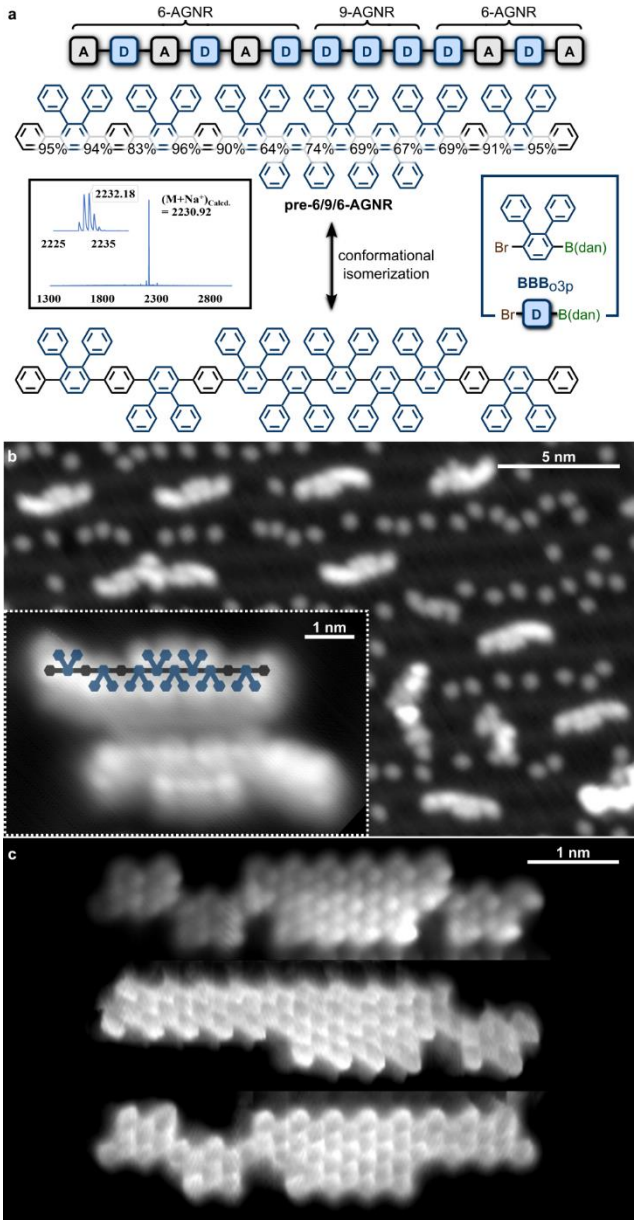

Figure 4. Double heterojunction: synthesis of **6/9/6-AGNRs.** (a) Synthesis of oligomer (GNR) precursor **pre-6/9/6-AGNR** demonstrating a 6/9/6 double heterojunction. Yields for each iteration in the oligomer synthesis are provided at the corresponding connecting positions. The inset shows MALDI-TOF-MS spectra of **pre-6/9/6-AGNR**. (b) Large-scale STM topograph (V = –2V, I = 50pA) of monodisperse oligomer (GNR) precursor (**pre-6/9/6-AGNRs**). The inset shows a close-up scan (V = –1.8V, I = 50pA) of two precursors, including structure overlay. (c) BRSTM images (constant height dI/dV at V = 0V) of **6/9/6-AGNRs** after CHD.

Kinked GNRs. Having established that the PAIS method can give access to length-controlled GNRs and precise sequence-defined GNR heterostructures, the potential of PAIS to generate GNRs with previously inaccessible shapes was investigated next. Our starting hypothesis was that GNRs with controlled angular turns could be obtained by selecting a BBB that has the bromine and B(dan) substituents at an angle relative to each other. "Kinked" GNRs termed **6-V-6-AGNR** (where the V represents the kink) were designed and synthesized by merging the **6-AGNR** scaffold with an *ortho*-phenylene unit (**BBB**$_{oph}$) (Figure 5a). The ortho linkage between the bromine and the B(dan) groups in **BBB**$_{oph}$ introduces an abrupt 120° growth direction change. After synthesis the oligomer (GNR) precursor (**pre-6-V-6-AGNR**) was transferred onto Au(111) using MAD for CDH and STM imaging. STM images (Figure 5b) and MALDI-TOF mass spectra (Figure 5a inset) corroborate

the correct V-shaped scaffold of the GNR oligomer precursors produced using PAIS. Figure 5c shows a large-scale image of mono-disperse **6-V-6-AGNRs** on Au(111) after CDH. Close-up BRSTM images can be seen in Figure 5d, which confirm that nearly all GNRs found on the surface have the expected 120-degree kink in their backbone, as well as the correct sequence and length. Similar to what was observed in the synthesis of **6/9/6-AGNR** heterostructures, conformational rotation at the **6-AGNR** segments also took place during the CDH stage, leading to flip isomers.

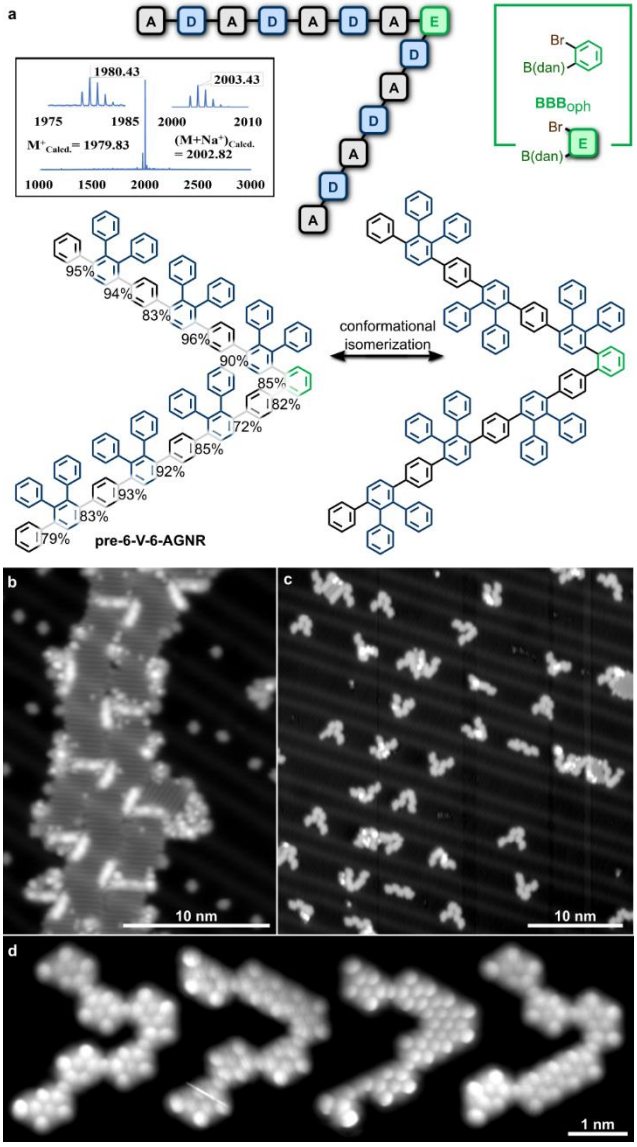

Figure 5. Kinked GNRs: synthesis of **6-V-6-AGNRs**. (a) Synthesis of oligomer (GNR) precursor **pre-6-V-6-AGNR** demonstrating a kinked GNR structure. Yields for each iteration in the oligomer synthesis are provided at the corresponding connecting positions. The inset shows MALDI-TOF-MS spectra of **pre-6-V-6-AGNRs**. (b) STM topograph (V = –1.4V, I = 100pA) of oligomer (GNR) precursor (**pre-6-V-6-AGNR**). (c) Large-scale STM topograph (V = –1.6V, I = 50pA) shows monodisperse **6-V-6-AGNRs** after CHD. (d) BRSTM images (constant height dI/dV at V = 0V) of **6-V-6-AGNRs**.

Lastly, to show the full range of structural flexibility afforded by PAIS the kinked structural motif was integrated into a two-component GNR heterostructure. This was accomplished by fabricating a kinked heterojunction using chevron and N=9 GNR building blocks. The new oligomeric precursor (**pre-9-V-chGNR**) was successfully prepared using the PAIS strategy (Figure 6a), involving the use of four different BBBs. Figures 6b and 6c show the GNR oligomer precursor after MAD deposition to the Au(111) surface. The chevron-GNR segments are in good agreement with previous images of regular chevron-GNR precursors,[8] while the 9-AGNR segments appear as bright lobes. Figure 6d shows a large-scale image of the

resulting monodisperse **9-V-chGNRs** after CDH. The close-up BRSTM images in Figure 6e show 120° kinked heterojunctions with a thick chevron arm bonded to a thinner N = 9 arm. Phenyl ejection defects are visible (similar to what was seen for **ch-GNR(6)** and **9-chGNR**) but the BRSTM images again confirm that the GNRs exhibit the exact sequence and length that they were designed to have.

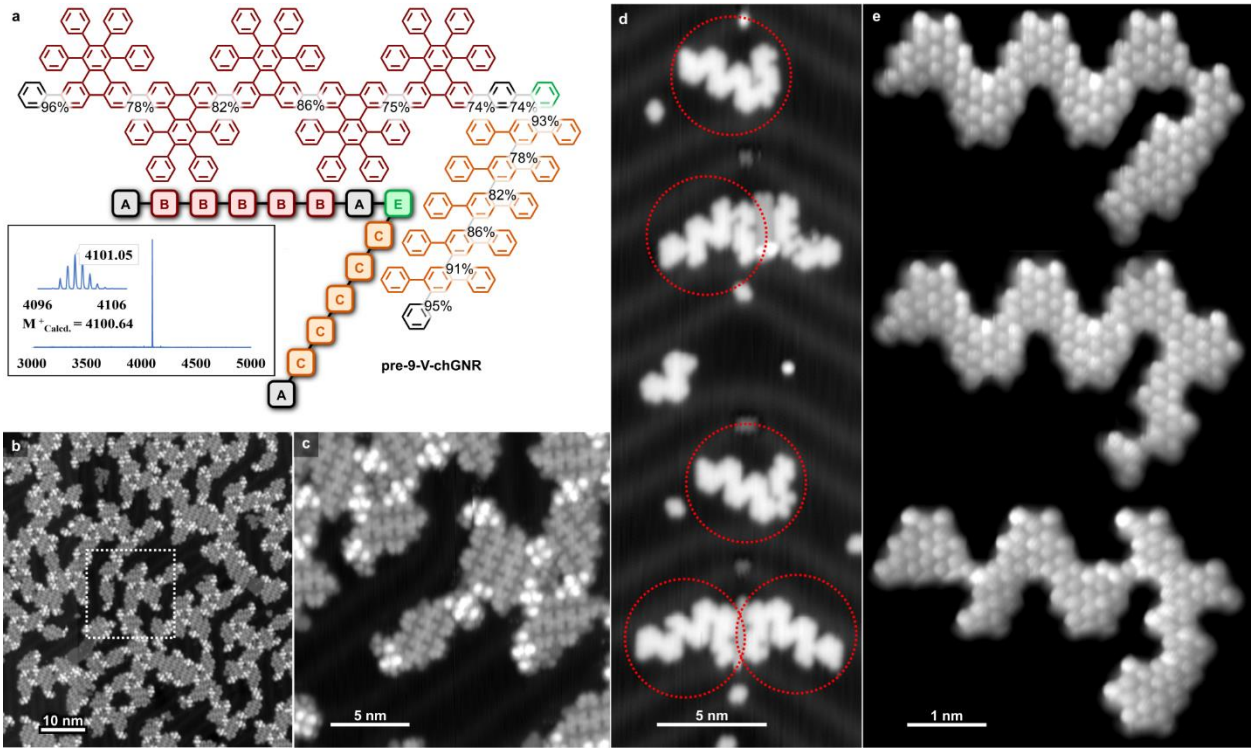

Figure 6. Kinked heterojunctions: synthesis of **9-V-chGNRs**. (a) Synthesis of oligomer (GNR) precursor **pre-9-V-chGNR** demonstrating a kinked, two-component GNR heterostructure. Yields for each iteration in the oligomer synthesis are provided at the corresponding connecting positions. The inset shows MALDI-TOF-MS spectra of **pre-9-V-chGNR**. (b) Large-scale STM topograph (V = –2V, I = 50pA) of oligomer (GNR) precursor (**pre-9-V-chGNRs**). (c) Close-up STM image (V = –2V, I = 50pA) of **pre-9-V-chGNR** (boxed area in **b**). (d) Large-scale STM topograph (V = –1.8V, I = 50pA) of monodisperse **9-V-chGNRs** after CHD (each GNR is labeled by a red circle). (e) BRSTM images (constant height dI/dV at V = 0V) of **9-V-chGNRs**.

CONCLUSION

In conclusion, we have developed a programmable approach to fabricate structurally diverse monodisperse GNRs with predetermined length, shape, and monomer sequence. This approach is enabled by the PAIS strategy, as well as subsequent MAD-transfer and on-surface CDH. The effectiveness and precision of the approach are supported by BRSTM characterization of diverse GNR structures that could not be fabricated using more conventional GNR synthesis techniques. While surface-induced CDH was used here to facilitate GNR characterization by STM, the PAIS strategy is not limited to on-surface synthesis. Utilization of this method for liquid-phase fabrication of longer and more complex monodisperse GNR structures is ongoing in our laboratories, which is also expected to address the scalability and some defect issues observed with the on-surface synthesis.

ASSOCIATED CONTENT

Supporting Information

The Supporting Information is available free of charge at

https://pubs.acs.org/doi/xx.xxxx/jacs.xxxxxxx.

Additional experimental details, materials, methods and spectral data (PDF)

AUTHOR INFORMATION

Corresponding Author

Guangbin Dong − Department of Chemistry, University of Chicago, Chicago, IL 60637, USA;

orcid.org/0000-0003-1331-6015; Email: gbdong@uchicago.edu

Michael F. Crommie − Department of Physics, University of California at Berkeley, Berkeley, CA 94720, USA. Materials Sciences Division, Lawrence Berkeley National Laboratory, Berkeley, CA 94720, USA. Kavli Energy NanoSciences Institute at the University of California, Berkeley and the Lawrence Berkeley National Labora-tory, Berkeley, CA 94720, USA. Email: crommie@berkeley.edu

Authors

Jiangliang Yin − Department of Chemistry, University of Chicago, Chicago, IL 60637, USA

Peter H. Jacobse − Department of Physics, University of California at Berkeley, Berkeley, CA 94720, USA; Materials Sciences Division, Lawrence Berkeley National Laboratory, Berkeley, CA 94720, USA

Daniel Pyle − Department of Chemistry, University of Chicago, Chicago, IL 60637, USA

Ziyi Wang − Department of Physics, University of California at Berkeley, Berkeley, CA 94720, USA; Materials Sciences Division, Lawrence Berkeley National Laboratory, Berkeley, CA 94720, USA

Author Contributions

[†]J.Y. and P.H.J. contributed equally.

Notes

A provisional patent application on the PAIS method has been filed.

ACKNOWLEDGMENTS

This research was supported by the Office of Naval Research MURI Program N00014-19-1-2596 (polymer design and synthesis, bond-resolved imaging), by the U.S. Department of Energy (DOE), Office of Science, Basic Energy Sciences (BES), under the Nanomachine Program award number DE-AC02-05CH11231 (MAD transfer, surface catalysis), and by the National Science Foundation grant DMR-1839098 (STM topography).

REFERENCES

(1) Wu, J.; Pisula, W.; Müllen, K. Graphenes as Potential Material for Electronics. *Chem. Rev.* **2007**, *107*, 718.
(2) Son, Y.-W.; Cohen M. L.; Louie, S. G. Half-Metallic Graphene Nanoribbons. *Nature* **2006**, *444*, 347.
(3) Li, X.; Wang, X.; Zhang, L.; Lee, S.; Dai, H. Chemically Derived, Ultrasmooth Graphene Nanoribbon Semiconductors. *Science* **2008**, *319*, 1229.
(4) Ritter, K. A.; Lyding, J. W. The Influence of Edge Structure on The Electronic Properties of Graphene Quantum Dots and Nanoribbons. *Nature Mater.* **2009**, *8*, 235.
(5) Prezzi, D.; Varsano, D.; Ruini, A.; Marini, A.; Molinari, E. Optical Properties of Graphene Nanoribbons: The Role of Many-Body Effects. *Phys. Rev. B* **2008**, *77*, 041404(R).
(6) Ruffieux, P.; Wang, S.; Yang, B.; Sánchez-Sánchez, C.; Liu, J.; Dienel, T.; Talirz, L.; Shinde, P.; Pignedoli, C. A.; Passerone, D.; Dumslaff, T.; Feng, X.; Müllen, K.; Fasel, R. On-Surface Synthesis of Graphene Nanoribbons with Zigzag Edge Topology. *Nature* **2016**, *531*, 489.
(7) Blackwell, R. E.; Zhao, F.; Brooks, E.; Zhu, J.; Piskun, I.; Wang, S.; Delgado, A.; Lee, Y.-L.; Louie, S. G.; Fischer, F. R. Spin Splitting of Dopant Edge State in Magnetic Zigzag Graphene Nanoribbons. *Nature*, **2021**, *600*, 647.
(8) Cai, J.; Ruffieux, P.; Jaafar, R.; Bieri, M.; Braun, T.; Blankenburg, S.; Muoth, M.; Seitsonen, A. P.; Saleh, M.; Feng, X.; Müllen, K.; Fasel, R. Atomically Precise Bottom-up Fabrication of Graphene Nanoribbons. *Nature*, **2010**, *466*, 470.
(9) Narita, A.; Wang, X.-Y.; Feng, X.; Müllen, K. New Advances in Nanographene Chemistry. *Chem. Soc. Rev.* **2015**, *44*, 6616.
(10) Narita, A.; Feng, X.; Müllen, K. Bottom-up Synthesis of Chemically Precise Graphene Nanoribbons. *Chem. Rec.* **2015**, *15*, 295.
(11) Talirz, L.; Ruffieux, P.; Fasel, R. On-Surface Synthesis of Atomically Precise Graphene Nanoribbons. *Adv. Mater.* **2016**, *28*, 6222.
(12) Houtsma, R. S. K.; de la Rie, J.; Stöhr, M. Atomically Precise Graphene Nanoribbons: Interplay of Structural and Electronic Properties. *Chem. Soc. Rev.* **2021**, *50*, 6541.
(13) Liu, Z.; Fu, S.; Liu, X.; Narita, A.; Samorì, P.; Bonn, M.; Wang, H. I. Small Size, Big Impact: Recent Progress in Bottom-Up

Synthesized Nanographenes for Optoelectronic and Energy Applications. *Advanced Science*, **2022**, 2106055.
(14) Zhou X.; Yu G. Modified Engineering of Graphene Nanoribbons Prepared via On-Surface Synthesis. *Adv. Mater.* **2020**, 32, 1905957.
(15) Yano, Y.; Mitoma, N.; Ito, H.; Itami, K. A Quest for Structurally Uniform Graphene Nanoribbons: Synthesis, Properties, and Applications. *J. Org. Chem.* **2020**, *85*, 4.
(16) Yoon, K.-Y.; Dong G. Liquid-Phase Bottom-Up Synthesis of Graphene Nanoribbons. *Mater. Chem. Front.* **2020**, 4, 29.
(17) Jolly, A.; Miao, D.; Daigle, M.; Morin, J.-F. Emerging Bottom-Up Strategies for The Synthesis of Graphene Nanoribbons and Related Structures. *Angew. Chem. Int. Ed.* **2020**, *59*, 4624.
(18) Han, P.; Akagi, K.; Federici Canova, F.; Mutoh, H.; Shiraki, S.; Iwaya, K.; Weiss, P. S.; Asao, N.; Hitosugi, T. Bottom-Up Graphene-Nanoribbon Fabrication Reveals Chiral Edges and Enantioselectivity. *ACS Nano* **2014**, 8, 9181.
(19) Kawai, S.; Nakatsuka, S.; Hatakeyama, T.; Pawlak, R.; Meier, T.; Tracey, J.; Meyer, E.; Foster, A. S. Multiple Heteroatom Substitution to Graphene Nanoribbon. *Sci. Adv.* **2018**, *4*, eaar7181.
(20) Xiao, X.; Pedersen, S. K.; Aranda, D.; Yang, J.; Wiscons, R. A.; Pittelkow, M.; Steigerwald, M. L.; Santoro, F.; Schuster, N. J.; Nuckolls, C. Chirality Amplified: Long, Discrete Helicene Nanoribbons. *J. Am. Chem. Soc.* **2021**, *143*, 983.
(21) For an elegant synthesis of monodisperse N-doped polyacenes, see: Cortizo-Lacalle, D.; Mora-Fuentes, J. P.; Strutyński, K.; Saeki, A.; Melle-Franco, M.; Mateo-Alonso, A. Monodisperse N-Doped Graphene Nanoribbons Reaching 7.7 Nanometers in Length. *Angew. Chem. Int. Ed.* **2018**, 57, 703. This approach is not suitable for preparing regular GNRs.
(22) (a) Yang, W.; Lucotti, A.; Tommasini, M.; Chalifoux, W. A. Bottom-Up Synthesis of Soluble and Narrow Graphene Nanoribbons Using Alkyne Benzannulations. *J. Am. Chem. Soc.* **2016**, *138*, 9137. (b) Hu, Y.; Xie, P.; De Corato, M.; Ruini, A.; Zhao, S.; Meggendorfer, F.; Straasø, L. A.; Rondin, L.; Simon, P.; Li, J.; Finley, J. J.; Hansen, M. R.; Lauret, J.-S.; Molinari, E.; Feng, X.; Barth, J. V.; Palma, C.-A.; Prezzi, D.; Müllen, K.; Narita, A. Bandgap Engineering of Graphene Nanoribbons by Control over Structural Distortion. *J. Am. Chem. Soc.* **2018**, *140*, 7803.
(23) Li, G.; Yoon, K.-Y.; Zhong, X.; Wang, J.; Zhang, R.; Guest, J. R.; Wen, J.; Zhu, X.-Y.; Dong, G. A Modular Synthetic Approach for Band-Gap Engineering of Armchair Graphene Nanoribbons. *Nat. Commun.* **2018**, *9*, 1687.
(24) Rizzo, D. J.; Veber, G.; Cao, T.; Bronner, C.; Chen, T.; Zhao, F.; Rodriguez, H.; Louie, S. G.; Crommie, M. F.; Fischer, F. R. Topological Band Engineering of Graphene Nanoribbons. *Nature* **2018**, *560*, 204.
(25) Cai, J.; Pignedoli, C. A.; Talirz, L.; Ruffieux, P.; Söde, H.; Liang, L.; Meunier, V.; Berger, R.; Li, R.; Feng, X.; Müllen, K.; Fasel, R. Graphene Nanoribbon Heterojunctions. *Nature Nanotech.* **2014**, *9*, 896.
(26) Nguyen, G. D.; Tsai, H.-Z.; Omrani, A. A.; Marangoni, T.; Wu, M.; Rizzo, D. J.; Rodgers, G. F.; Cloke, R. R.; Durr, R. A.; Sakai, Y.; Liou, F.; Aikawa, A. S.; Chelikowsky, J. R.; Louie, S. G.; Fischer, F. R.; Crommie, M. F. Atomically Precise Graphene Nanoribbon Heterojunctions from a Single Molecular Precursor. *Nat. Nanotech.* **2017**, *12*, 1077.
(27) Jacobse, P. H.; Kimouche, A.; Gebraad, T.; Ervasti, M. M.; Thijssen, J. M.; Liljeroth, P.; Swart, I. Electronic Components Embedded in a Single Graphene Nanoribbon. *Nat. Commun.* **2017**, *8*, 119.
(28) Chen, Y.-C.; Cao, T.; Chen, C.; Pedramrazi, Z.; Haberer, D.; de Oteyza, D. G.; Fischer, F. R.; Louie, S. G.; Crommie, M. F. Molecular Bandgap Engineering of Bottom-up Synthesized Graphene Nanoribbon Heterojunctions. *Nature Nanotech.* **2015**, *10*, 156.
(29) Bronner, C.; Durr, R. A.; Rizzo, D. J.; Lee, Y.-L.; Marangoni, T.; Kalaylian, A. M.; Rodriguez, H.; Zhao, W.; Louie, S. G.; Fischer, F. R.; Crommie, M. F. Hierarchical On-Surface Synthesis of Graphene Nanoribbon Heterojunctions. *ACS Nano* **2018**, *12*, 2193.
(30) Bennett, P. B.; Pedramrazi, Z.; Madani, A.; Chen, Y.-C.; de Oteyza, D. G.; Chen, C.; Fischer, F. R.; Crommie, M. F.; Bokor, J. Bottom-up Graphene Nanoribbon Field-Effect Transistors. *Appl. Phys. Lett.* **2013**, *103*, 253114.
(31) Areshkin, D. A.; White, C. T. Building Blocks for Integrated Graphene Circuits. *Nano Lett.* **2007**, *7*, 3253.
(32) Gröning, O.; Wang, S.; Yao, X.; Pignedoli, C. A.; Borin Barin, G.; Daniels, C.; Cupo, A.; Meunier, V.; Feng, X.; Narita, A.; Müllen, K.; Ruffieux, P.; Fasel, R. Engineering of Robust Topological Quantum Phases in Graphene Nanoribbons. *Nature* **2018**, *560*, 209.
(33) Lee, Y. L.; Zhao, F.; Cao, T.; Ihm, J.; Louie, S. G. Topological Phases in Cove-Edged and Chevron Graphene Nanoribbons: Geometric Structures, Z2 Invariants, and Junction States. *Nano Lett.* **2018**, *18*, 7247.
(34) Sun, Q.; Gröning, O.; Overbeck, J.; Braun, O.; Perrin, M. L.; Borin Barin, G.; El Abbassi, M.; Eimre, K.; Ditler, E.; Daniels, C.; Meunier, V.; Pignedoli, C. A.; Calame, M.; Fasel, R.; Ruffieux, P. Massive Dirac Fermion Behavior in a Low Bandgap Graphene Nanoribbon Near a Topological Phase Boundary. *Adv. Mater.* **2020**, *32*, 1906054.
(35) Li, J.; Sanz, S.; Merino-Díez, N.; Vilas-Varela, M.; Garcia-Lekue, A.; Corso, M.; de Oteyza, D. G.; Frederiksen, T.; Peña, D.; Pascual, J. I. Topological Phase Transition in Chiral Graphene Nanoribbons: From Edge Bands to End States. *Nat. Commun.* **2021**, *12*, 5538.
(36) Rizzo, D. J.; Veber, G.; Jiang, J.; McCurdy, R.; Cao, T.; Bronner, C.; Chen, T.; Louie, S. G.; Fischer, F. R.; Crommie, M. F. Inducing Metallicity in Graphene Nanoribbons via Zero-Mode Superlattices. *Science* **2020**, *369*, 1597.
(37) Li, J.; Sanz, S.; Corso, M.; Choi, D. J.; Peña, D.; Frederiksen, T.; Pascual, J. I. Single Spin Localization and Manipulation in Graphene Open-Shell Nanostructures. *Nat. Commun.* **2019**, *10*, 200.
(38) Wang, T.; Sanz, S.; Castro-Esteban, J.; Lawrence, J.; Berdonces-Layunta, A.; Mohammed, M. S. G.; Vilas-Varela, M.; Corso, M.; Peña, D.; Frederiksen, T.; de Oteyza, D. G. Magnetic Interactions Between Radical Pairs in Chiral Graphene Nanoribbons. *Nano Lett.* **2022**, *22*, 164.
(39) Chen, C.-C.; Chang, Y.-C. Theoretical Studies of Graphene Nanoribbon Quantum Dot Qubits. *Phys. Rev. B* **2015**, *92*, 245406.
(40) Grichuk, E. S.; Manykin, E. A. Spin Polarized Quantum Pump Effect in Zigzag Graphene Nanoribbons. *JETP Lett.* **2011**, *93*, 372.
(41) Zamani, S.; Farghadan, R. Graphene Nanoribbon Spin-Photodetector. *Phys. Rev. Appl.* **2018**, *10*, 34059.
(42) Slota, M.; Keerthi, A.; Myers, W. K.; Tretyakov, E.; Baumgarten, M.; Ardavan, A.; Sadeghi, H.; Lambert, C. J.; Narita, A.; Müllen, K.; Bogani, L. Magnetic Edge States and Coherent Manipulation of Graphene Nanoribbons. *Nature* **2018**, *557*, 691.
(43) Guo, G.; Lin, Z.; Li, X.; Tu, T. Quantum Computation with Graphene Nanoribbon. *New J. Phys.* **2009**, *11*, 123005.
(44) Gani, Y. S.; Abergel, D. S. L.; Rossi, E. Electronic Structure of Graphene Nanoribbons on Hexagonal Boron Nitride. *Phys. Rev. B* **2018**, *98*, 205415.
(45) Klinovaja, J.; Loss, D. Giant Spin-Orbit Interaction Due to Rotating Magnetic Fields in Graphene Nanoribbons. *Phys. Rev. X* **2013**, *3*, 11008.

(46) Wang, S.; Kharche, N.; Costa Girão, E.; Feng, X.; Müllen, K.; Meunier, V.; Fasel, R.; Ruffieux, P. Quantum Dots in Graphene Nanoribbons. *Nano Lett.* **2017**, *17*, 4277..
(47) Lafferentz, L.; Eberhardt, V.; Dri, C.; Africh, C.; Comelli, G.; Esch, F.; Hecht, S.; Grill, L. Controlling On-Surface Polymerization by Hierarchical and Substrate-Directed Growth. *Nat. Chem.* **2012**, *4*, 215.
(48) von Kugelgen, S.; Piskun, I.; Griffin, J. H.; Eckdahl, C. T.; Jarenwattananon, N. N.; Fischer, F. R. Templated Synthesis of End-Functionalized Graphene Nanoribbons through Living Ring-Opening Alkyne Metathesis Polymerization. *J. Am. Chem. Soc.* **2019**, *141*, 11050.
(49) Yoon, Y.; Salahuddin S. Barrier-Free Tunneling in a Carbon Heterojunction Transistor, *Appl. Phys. Lett.* **2010**, *97*, 033102.
(50) Caruthers, M. H. Gene Synthesis Machines: DNA Chemistry and Its Uses. *Science* **1985**, *230*, 281.
(51) When this manuscript was in preparation, the use of MIDA boronate groups in sequence-controlled polymer synthesis was reported; but this method is not suitable for GNR oligomer preparations due to the relative instability and poor solubility of MIDA moiety: Xu, C.; He, C.; Li, N.; Yang, S.; Du, Y.; Matyjaszewski, K.; Pan, X. Regio- and Sequence-Controlled Conjugated Topological Oligomers and Polymers via Boronate-Tag Assisted Solution-Phase Strategy. *Nat. Commun.* **2021**, *12*, 5853.
(52) Noguchi, H.; Hojo, K.; Suginome, M. Boron-masking Strategy for the Selective Synthesis of Oligoarenes via Iterative Suzuki-Miyaura Coupling. *J. Am. Chem. Soc.* **2007**, *129*, 758.
(53) McCurdy, R. D.; Jacobse, P. H.; Piskun, I.; Veber, G. C.; Rizzo, D. J.; Zuzak, R.; Mutlu, Z.; Bokor, J.; Crommie, M. F.; Fischer, F. R. Synergetic Bottom-Up Synthesis of Graphene Nanoribbons by Matrix-Assisted Direct Transfer. *J. Am. Chem. Soc.* **2021**, *143*, 4174.
(54) Costa, P. S.; Teeter, J. D.; Enders, A.; Sinitskii, A. Chevron-Based Graphene Nanoribbon Heterojunctions: Localized Effects of Lateral Extension and Structural Defects on Electronic Properties. *Carbon* **2018**, *134*, 310.
(55) Pizzochero, M.; Čerņevičs, K.; Borin Barin, G.; Wang, S.; Ruffieux, P.; Fasel, R.; Yazyev, O. V. Quantum Electronic Transport across 'Bite' Defects in Graphene Nanoribbons. *2D Mater.* **2021**, *8*, 035025.
(56) Li, G.; Yoon, K.-Y.; Zhong, X.; Zhu, X.; Dong, G. Efficient Bottom-Up Preparation of Graphene Nanoribbons by Mild Suzuki–Miyaura Polymerization of Simple Triaryl Monomers. *Chem. Eur. J.* **2016**, *22*, 9116.
(57) Talirz, L.; Söde, H.; Dumslaff, T.; Wang, S.; Sanchez-Valencia, J. R.; Liu, J.; Shinde, P.; Pignedoli, C. A.; Liang, L.; Meunier, V.; Plumb, N. C.; Shi, M.; Feng, X.; Narita, A.; Müllen, K.; Fasel, R.; Ruffieux, P. On-Surface Synthesis and Characterization of 9-Atom Wide Armchair Graphene Nanoribbons. *ACS Nano* **2017**, *11*, 1380.

programmable fabrication of monodisperse GNRs